

# Mass reconstruction and noise reduction with cosmic-web environments

Feng Fang<sup>1</sup>, Yan-Chuan Cai<sup>2,\*</sup>, Zhuoyang Li<sup>1,3</sup>, Shiyu Yue<sup>1</sup>, Weishan Zhu<sup>1</sup>, and Longlong Feng<sup>1†</sup>

<sup>1</sup>*School of Physics and Astronomy, Sun Yat-Sen University, Zhuhai 519082, China*

<sup>2</sup>*Institute for Astronomy, University of Edinburgh, Blackford Hill, Edinburgh, EH9 3HJ, UK*

<sup>3</sup>*Department of Astronomy, Tsinghua University, Beijing 100084, China*

(Dated: November 28, 2023)

The clustering of galaxies and their connections to their initial conditions is a major means by which we learn about cosmology. However, the stochasticity between galaxies and their underlying matter field is a major limitation for precise measurements of galaxy clustering. It also hinders accurate mass reconstruction for retrieving cosmological information from observations. Efforts have been made with an optimal weighting scheme to reduce this stochasticity using the mass-dependent clustering of dark matter halos, but its application to observation is challenging due to the difficulties in measuring the mass of halos precisely. Here, we show that this is not optimal. We demonstrate that the cosmic-web environments (voids, sheets, filaments & knots) of halos provide extra information for reducing stochasticity. Using the environmental information alone can increase the signal-to-noise of clustering by approximately a factor of 3, better than the Poisson level at the scales of the baryon acoustic oscillations. This improvement is comparable to using halo mass information alone. The information about the environment and halo mass are complementary. Their combination increases the signal-to-noise by another factor of 2-3. The information about the cosmic web correlates with other properties of halos, including halo concentrations and tidal forces, thus, these are among the most dominant factors that can help improve the reconstruction. We attribute the extra information from the environment and secondary properties of halos primarily to the assembly bias of halos. Our findings open a new avenue for mass reconstruction and noise reduction using information beyond the halo mass.

A major challenge in cosmology with large-scale structure is to reconstruct the initial conditions from observations of the late-time Universe. While the initial matter density field is thought to be linear and continuous, what we observe in the late-time Universe is a discrete sampling of a non-linear matter field, typically traced out by galaxies. The accuracy of the reconstruction determines the amount of cosmological information we can extract from observations. It can be quantified with the correlation coefficient  $r$  between the galaxy number density field  $\delta_g$  and the matter density field  $\delta_m$ ,

$$r \equiv \frac{\langle \delta_g \delta_m \rangle}{\sqrt{\langle \delta_g^2 \rangle \langle \delta_m^2 \rangle}}. \quad (1)$$

The  $\langle \rangle$  symbol denotes the ensemble average. To the first order, galaxies are linearly biased against matter. With the presence of shot noise  $\epsilon$ , we have  $\delta_g = b\delta_m + \epsilon$ , where  $b$  is the linear bias of galaxies. With  $\langle \epsilon \delta_m \rangle = 0$ , we have  $P_g = \langle \delta_g^2 \rangle = b^2 P_m + \langle \epsilon^2 \rangle$ ,  $P_{gm} = \langle \delta_g \delta_m \rangle = b P_m$ , where  $P_m$  is the matter power spectrum; and so

$$\frac{\langle \epsilon^2 \rangle}{b^2 P_m} = \frac{1 - r^2}{r^2}. \quad (2)$$

All the above quantities are functions of the Fourier number  $k$ . We can see that the presence of the noise, or stochasticity, degrades the correlation coefficient  $r$  [1–3]. Minimizing stochasticity, increasing correlation coefficients and optimizing mass reconstruction are different sides of the same coin. Reducing  $\epsilon$  has the following observational implications:

(1) increasing the signal-to-noise ratio for the clustering of galaxies [e.g. 3–5], which is particularly beneficial for analyses of the baryon acoustic oscillations (BAO) with sparse tracers [e.g. 6–13];

(2) increasing the correlations between the galaxy field and the matter field, allowing more cosmological information to be retrieved from the measurement of galaxy-galaxy lensing and reconstruction [e.g. 14–19].

If  $\epsilon$  is Poissonian, its power spectrum is  $1/\bar{n}$ , with  $\bar{n}$  being the number density of tracers. Recent work has shown that we can improve beyond the Poisson limit [3–5, 14, 20–23]. In N-body simulations where the masses of dark matter halos are known, [5] and [3] have shown that a linear combination of halos of different masses with different weights can significantly reduce stochasticity. The primary information used for the improvement is the mass-dependence of halo power spectra  $P_h(k, M)$ , where  $M$  is the mass of halos. One way to understand this is that the linear halo bias  $b(M)$  increases with  $M$ ; for the same number of halos, the signal-to-noise of  $P_h(k, M)$  is higher for halos with larger masses. Therefore, it is preferable to up-weight the high-mass halos to increase the signal-to-noise. This is indeed the case for the optimal weights found in [3, 5].

However, this can not be the full physical picture. In addition to  $M$ , the clustering of halos depends also on other secondary properties. Among them, the formation time of halos is known to affect the halo clustering. For low-mass halos, those who formed earlier tend to exhibit stronger clustering than younger ones. This is known as the halo assembly bias [24, 25]. This indicates that there

is room for further improvement in the reconstruction if this secondary property of halos can be used, and it is the focus of this letter.

A main challenge for this is that the formation time of halos or galaxies is difficult to measure in observations. However, it is known to correlate with other properties of halos, especially with halo concentration, tidal force, and their cosmic-web environments [e.g. 26–28], with some arguing that cosmic-web anisotropy is the main indicator for halo assembly bias [29–31], the latter is accessible in observations. We will, therefore, focus on using the cosmic-web environment for the reconstruction.

Suppose we have an observed halo number density field, denoted as  $\delta_h$ ; It is a discrete sampling of its underlying matter field  $\delta_m$ . Our aim is to maximize the correlation coefficient  $r$  between these two fields, defined in equation (1), substituting the subscript  $b$  by  $h$  to represent halos. We can see that  $r$  is agnostic about the linear halo bias. When  $r = 1$ , perturbation modes are in phase, but their amplitudes can be different.

To maximize  $r$ , we split the halo catalog  $n_h$  into  $N_s$  sub-samples with  $n_{hi} = \sum_{i=1}^{N_s} n_i$ , and weight each sub-sample with  $W_i \in \mathbb{R}$ . We then combine these weighted sub-samples to obtain the reconstructed density field  $n_c = \sum_i^{N_s} W_i n_i$ . The  $i$ th sub-sample can be written as  $n_i = \sum_{j=1}^{N_i} w_j \delta_D(\vec{x} - \vec{x}_j)$ , where  $\delta_D$  is the Dirac delta function and  $w_j$  represents the initial weight of each tracer, which could be the selection function in observation or the halo mass in simulation, and  $N_i$  is the number of halos in the  $i$ th sub-sample. Thus, the overdensity of the reconstructed fields  $\delta_c$  is

$$\delta_c \equiv \frac{n_c}{\bar{n}_c} - 1 = \frac{\sum_i^{N_s} W_i \bar{n}_i (1 + \delta_i)}{\sum_i^{N_s} W_i \bar{n}_i} - 1 = \boldsymbol{\omega}^T \boldsymbol{\delta}, \quad (3)$$

where  $\boldsymbol{\omega}$  and  $\boldsymbol{\delta}$  are  $N_s$ -vectors, with elements  $\omega_i = \frac{W_i \bar{n}_i}{\sum W_i \bar{n}_i}$  and  $\delta_i = \frac{n_i}{\bar{n}_i} - 1$  respectively. Combining equations (1) and (3), we have:

$$r_c^2 = \frac{\sum_{ij} \omega_i B_{ij} \omega_j}{\sum_{ij} \omega_i C_{ij} \omega_j} = \frac{\boldsymbol{\omega}^T \mathbf{B} \boldsymbol{\omega}}{\boldsymbol{\omega}^T \mathbf{C} \boldsymbol{\omega}}, \quad (4)$$

with the symmetric matrices  $\mathbf{B}$  and  $\mathbf{C}$  defined as

$$\begin{cases} B_{ij} = \frac{\langle \delta_i \delta_m \rangle \langle \delta_j \delta_m \rangle}{\langle \delta_m \delta_m \rangle}, \\ C_{ij} = \langle \delta_i \delta_j \rangle. \end{cases} \quad (5)$$

To solve for the weights that maximize  $r_c^2$ , we set the derivative of  $r_c^2$  to be 0 to obtain:

$$\mathbf{B} \boldsymbol{\omega} = r_c^2 \mathbf{C} \boldsymbol{\omega}. \quad (6)$$

The above eigenvalue equation (6) is a generalized eigen-problem that can be solved numerically. We use the linear algebra library LAPACK[32]::dspgv() to do this. The square root of the maximum eigenvalue corresponds

to the maximum correlation coefficient, and the corresponding normalized eigenvector represents the optimal weight  $\boldsymbol{\omega}$ . The key information needed for solving the above equation is the matrices of  $\mathbf{C}$  and  $\mathbf{B}$ . These can be measured from N-body simulations.

In summary, our method for the reconstruction is to maximize the correlation coefficients between the halo field and the matter density field. To do that, we make a linear combination of the tracers; each is given a weight. We can solve for the weights  $\boldsymbol{\omega}$  that maximize the correlation coefficients. The above derivation follows closely that of [3] but using a different target function  $r^2$ . The results agree with each other. The derivation is general i.e., given any field of tracers, which can be dark matter haloes, galaxies, or HI field, and its underlying matter field  $\delta_m$ , we can solve equation (6) to find the optimal  $\boldsymbol{\omega}$  that maximizes  $r_c$ . Next, we will apply this method to halos in simulations, using information about their cosmic-web environment.

We use the public MULTIDARK MDPL2 simulations [33] and their corresponding ROCKSTAR halo catalogues [34] for our analysis. The simulation is run with 3840<sup>3</sup> particles in a box of  $1 h^{-1} \text{Gpc}$  following a flat  $\Lambda \text{CDM}$  model with  $\Omega_m = 0.307, \Omega_b = 0.048, h = 0.678, n_s = 0.96, \sigma_8 = 0.823$ . We use a sample of  $\sim 2.37 \times 10^6$  halos with the minimal halo mass of  $2.0 \times 10^{12} h^{-1} M_\odot$ .

We first split the halos sample into equal-number bins according to their masses. We then further split each mass bin according to their cosmic-web environment—voids, sheets, filaments, and knots. We define the environment using the Hessian of the gravitational potential [26, 35] smoothed at  $1 h^{-1} \text{Mpc}$ . The three eigenvalues of the field ( $\lambda_{1,2,3}$ ) are compared with a threshold value  $\lambda_{\text{th}}$  to classify each volume as voids ( $\lambda_{1,2,3} < \lambda_{\text{th}}$ ), sheets ( $\lambda_{1,2} < \lambda_{\text{th}} < \lambda_3$ ), filaments ( $\lambda_1 < \lambda_{\text{th}} < \lambda_{2,3}$ ), and knots ( $\lambda_{\text{th}} < \lambda_{1,2,3}$ ) [35]. The threshold value of  $\lambda_{\text{th}}$  is a free parameter that will be commented later. With this, the halo sample is split into four environmental bins according to their host cosmic-web environment. So, the halo field has two dependencies, mass  $M$  and environment  $Env$ . The auto- and cross-correlations of  $\delta_h(M, Env)$  form the matrix of  $\mathbf{C}$  needed in equation (6). We have four bins of the environment by definition. If we choose four mass bins,  $\mathbf{C}$  will be a matrix of  $16 \times 16$ . Its correlation with the matter density field  $\delta_m$  yields the matrix  $\mathbf{B}$ . These will be inserted into equation (6) to find the maximum  $r_c$  and the optimal weights  $\boldsymbol{\omega}$ .

Figure 1 presents comparisons of scatter plots between the dark matter density field versus the reconstructed halo field with different weights. We can see that the scatter is the largest when halos are weighted equally (panel A), followed by mass-weighting (panel B), and then the optimization with cosmic-web information (panel C). It is clear that by optimizing with the cosmic-web information, we can reduce the stochasticity to a level which is comparable with the mass weighting case. Panel D shows

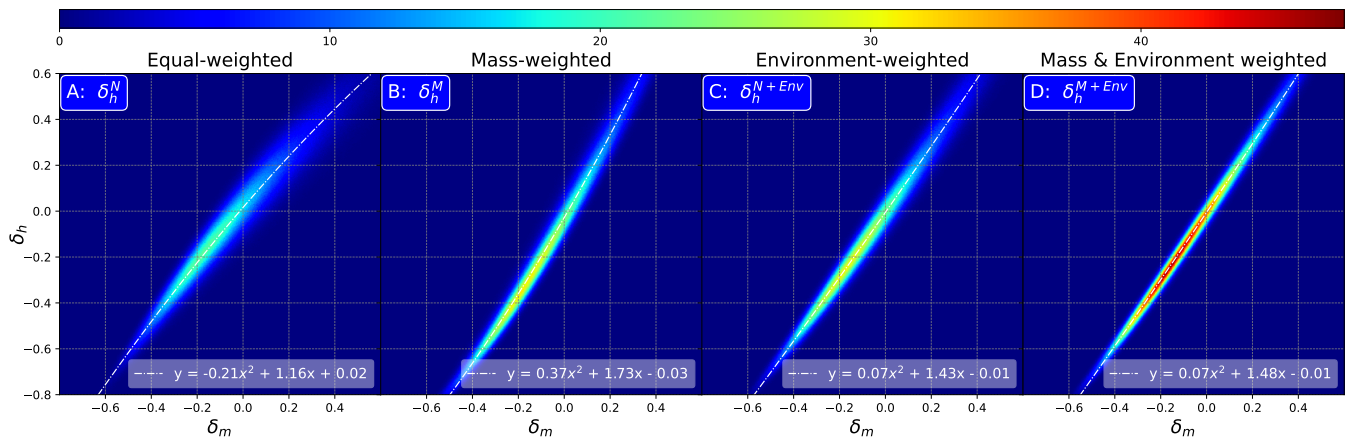


FIG. 1. Joint probability density distributions of matter density fields  $\delta_m$  and reconstructed halo density field with different weights. Each panel contains a random sampling of  $\sim 10^7$  points within the simulation box, smoothed by a top-hat filter with the radius of  $R = 30 h^{-1}\text{Mpc}$ . The colorbar indicates the particle number density. Panel A: halo number density  $\delta_h^N$  (equal weighting) versus  $\delta_m$ . B: Mass-weighted halo density  $\delta_h^M$  versus  $\delta_m$ . C: Optimal-environmental weighted halo density  $\delta_h^{N+Env}$  versus  $\delta_m$ . D:  $\delta_h^{M+Env}$  versus  $\delta_m$ : optimally weighted halo density field with four halo mass bins and four environmental bins. The threshold parameter for the environmental split has been optimized, with  $\lambda_{\text{th}} = 11.25$  and  $17.5$  for C and D, respectively. See also Figure 3 and the main text for the details. Quadratic fits with the best-fit parameters shown in the legends.

the result from optimizing with  $M$  and  $Env$ , which reduces the stochasticity further to achieve the lowest level of all. Therefore, the information from  $M$  and  $Env$  are complementary. Their combination is better than having each of them alone.

It is also worth noting that the mean correlation relation between the halo field and the mass field, which is the deterministic component of the bias, also tends to be more linear for the optimal weighting cases i.e., having the smallest quadratic coefficient  $b_2$  when fitted with a second-order polynomial function ( $b_2 = -0.21, 0.37, 0.07, 0.07$  for the four cases shown in the legend of the figure). This suggests that the second-order bias of halos is suppressed by the optimization – an unexpected but preferable outcome. This is consistent with the results report in [3].

The reduction of scatter in Figure 1 can be translated into an increase of signal-to-noise for halo clustering. The upper panel of Figure 2 compares the noise spectra for the above four cases. Note that the Poisson noise levels are different for different weighting schemes. We can see that except equal-weighting where  $\langle \epsilon^2 \rangle$  is comparable to Poisson noise, all the other noise spectra are below their Poisson noise levels. By weighting with the cosmic-web environment (orange line), we are able to bring the noise level down below the case of mass weighting (green line). When we incorporate both  $M$  and  $Env$  for the optimization, the noise level is the lowest, approximately one order of magnitude below the Poisson level. This is  $\sim 75\%$  lower than using the information of  $M$  alone.

The lower panel of Figure 2 compares  $\langle \epsilon^2 \rangle / (b^2 P_m)$  – the fractional errors on the power spectra, or the ‘noise-to-signal’, for all the four cases. This is directly related

to  $r_c$  through equation (2). We can see again that environmental weighting alone is comparable to mass weighting. They are approximately three times lower than equal weighting at low- $k$ ’s where the baryon acoustic oscillations are. Optimizing with both  $M$  and  $Env$  reduces the ratio further by another factor of  $\sim 2$ -3. The optimal weighting is thus expected to increase the signal-to-noise ratio of halo clustering by the same amount in the regime where shot-noise dominates.

The level of improvement for the reconstruction by having the information about the environment depends on the number of halo mass bins  $M_{\text{bin}}$  and the threshold value  $\lambda_{\text{th}}$  for the cosmic-web classification. We discuss these two variables as follows.

For a fixed  $M_{\text{bin}}$ ,  $r_c$  varies with  $\lambda_{\text{th}}$ , as shown in orange and red lines in Figure 3. There is an optimal  $\lambda_{\text{th}}$  at which  $r_c$  is maximized. We find that the optimal  $\lambda_{\text{th}}$  is typically larger than zero. This makes both the volume fraction for voids and the number of halos classified as void-halos to be the largest, followed by sheets, filaments, and knots (see also figures in Supplementary Material and [26, 35]). We have optimized  $\lambda_{\text{th}}$  for results in the paper unless specified. We present the best-fit functions for the optimal  $\lambda_{\text{th}}$  versus  $M_{\text{bin}}$  and the corresponding  $r_c$  versus  $M_{\text{bin}}$  in Supplementary Material.

With the optimal  $\lambda_{\text{th}}$ ,  $r_c$  increases with increasing  $M_{\text{bin}}$  (horizontal lines in Figure 3). When  $M_{\text{bin}}$  is large, each individual halo is effectively in a single bin. All properties of halos are used in the optimization, leaving no room for further improvement. In the other extreme case where no information about the halo mass is known, i.e.,  $M_{\text{bin}} = 1$ , the improvement for the reconstruction with the cosmic-web information is maximized. This is illus-

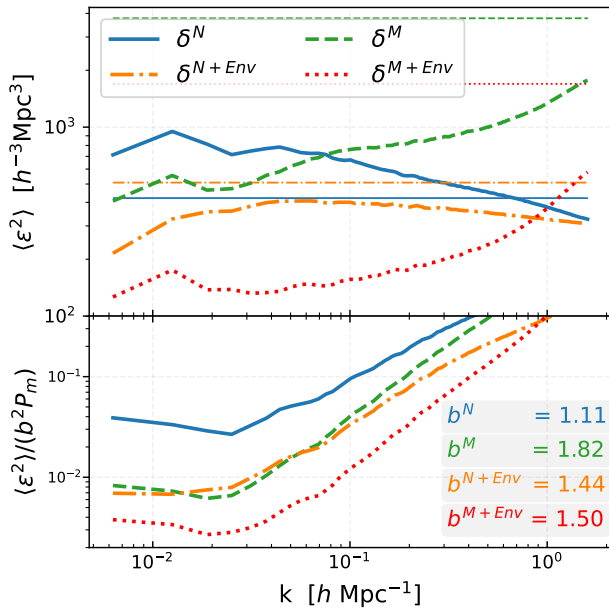


FIG. 2. Upper panel: the power spectra of the noise  $\langle \epsilon^2 \rangle = \langle (b\delta_m - \delta_h)^2 \rangle$  for the four reconstructed halo fields shown in Figure 1 and labeled in the legend.  $\delta_h^N$ : equal weighting;  $\delta_h^M$ : mass weighting;  $\delta_h^N + Env$ : environmental weighting;  $\delta_h^{M+Env}$ : optimal mass and environmental weighting. Their corresponding Poisson noise levels are shown in horizontal lines of the same color. Bottom: the corresponding fractional errors on the power spectra, or the ‘noise-to-signal’ ratio  $\langle \epsilon^2 \rangle / (b^2 P_m)$ , see also equation (2).

trated in Figure 3 by the length of the blue vertical line in terms of the correlation coefficient  $r_c$ . We can see that equal-weighting provides the lowest  $r_c$  (gray dashed line, labeled as  $N$ ); using the cosmic-web information alone (orange line, labeled as  $N + Env$ ) significantly improves  $r_c$ , and slightly outperforms the mass weighting case (labeled as  $M$ ); having two or more mass bin for the optimization increases  $r_c$  further.  $r_c = 0.99$  is achieved by having one mass bin and the environment information ( $M + Env$ , red-solid line). This is approximately the same as having 16 mass bins ( $M-16$ ) for optimization. Note that having many mass bins is unrealistic, given the challenge of measuring the mass of halos in observations. The gain we can achieve using the cosmic-web information is, therefore, highly complementary.

It is worth noting that when optimizing with the mass information, we assume that the mass of each individual halo is known. This is unrealistic in practice. We anticipate large uncertainties for estimating halo mass in real observations. Therefore, the benefit of using environmental weighting may be more prominent than we have shown.

In summary, we have found significant improvement for the correlation between halos and their underlying mass

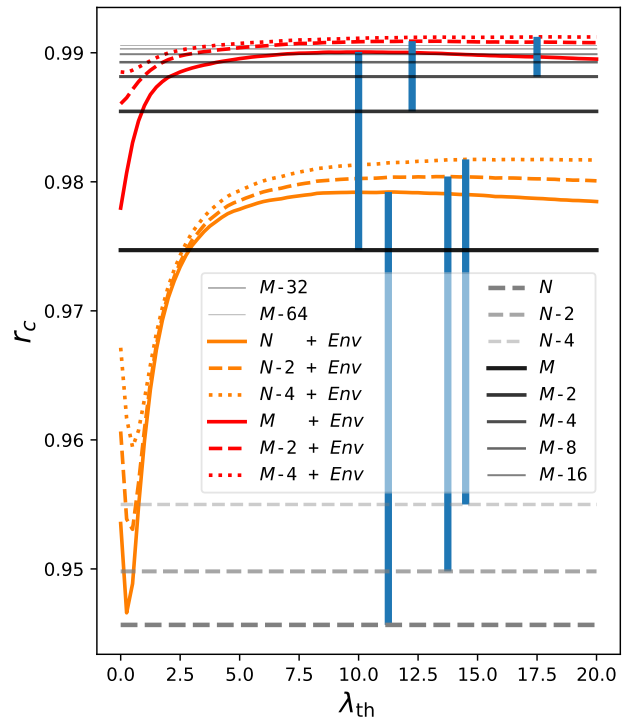


FIG. 3. The correlation coefficient  $r_c$  between the matter density and reconstructed fields versus the threshold value  $\lambda_{th}$  for cosmic-web classification. Orange lines ( $N$ ): equal-weighting plus environmental weighting; red lines ( $M$ ): mass-weighting plus environmental weighting. The horizontal lines of dashed gray and solid black represent results from mass weighting and equal weighting only respectively, without any environmental information. Blue vertical lines indicate the peak  $r_c$  values, Their length indicates the impact of the environment. The measurements are performed in configuration space with a  $R = 15 h^{-1} \text{Mpc}$  top-hat smoothing.

field using information about the cosmic-web environment. The level of improvement for the reconstruction is at least as good as optimizing using halo mass. Environment and halo mass complement each other. Their combination yields the best reconstruction than having each of them individually. Our findings have direct observational implications.

Reducing stochasticity, or noise, for the galaxy/halo population will directly increase the signal-to-noise for galaxy clustering. This is crucial for precise measurement of the BAO, especially at high redshifts where the tracers are sparse [e.g. 6, 8–11, 13]. Galaxy redshift surveys such as BOSS [36], eBOSS [37] and DESI [38], are designed to target at a specific type of galaxy, such as LRG, galaxies with approximately constant stellar mass, and emission line galaxies, but it is challenging to know the mass of individual halos. This limits the potential of shot-noise reduction using the halo mass information. In contrast, the cosmic-web information is more readily available from

computing the Hessian matrix using the galaxy samples themselves. A caveat is that the smoothing scale will be limited by the number density of galaxies, but we have tested using a relatively large smoothing scale ( $R = 5 h^{-1} \text{Mpc}$ ) to define the cosmic web, and there is still an obvious gain of information. An additional challenge is that the observed galaxies are in redshift space and so the defined cosmic web may be different from its real-space version. Further investigations are needed to fully realize the strength of the method in observations.

Reducing stochasticity between galaxies/halos versus the matter field also has direct benefits for forward modeling e.g. BORG [39], constrained simulations [e.g. 40], and cosmological inference at the field level using observations of the large-scale structure [e.g. 41, 42]. The common starting point for the above analyses is the observed galaxy number density field  $\delta_g$ , one then try to find the initial matter density field  $\delta_m^i$  which, after non-linear evolution, may generate the observed  $\delta_g$ . Reducing stochasticity for  $\delta_g$  will directly reduce the errors between the observational constraints with their initial conditions. Our method opens a promising path for achieving this.

We are aware that the environment is not the only secondary property of halos that can be useful for reconstruction. We have explored all other halo properties typically defined in N-body simulations, finding that information from the tidal force and halo concentration can also help to improve the reconstruction. This is expected as these halo properties are correlated and are all related to the assembly bias of halos [e.g. 26, 28].

## ACKNOWLEDGEMENTS

The CosmoSim database used in this paper is a service by the Leibniz-Institute for Astrophysics Potsdam (AIP). The MultiDark database was developed in cooperation with the Spanish MultiDark Consolider Project CSD2009-00064. The authors gratefully acknowledge the Gauss Centre for Supercomputing e.V. ([www.gauss-centre.eu](http://www.gauss-centre.eu)) and the Partnership for Advanced Supercomputing in Europe (PRACE, [www.prace-ri.eu](http://www.prace-ri.eu)) for funding the MultiDark simulation project by providing computing time on the GCS Supercomputer SuperMUC at Leibniz Supercomputing Centre (LRZ, [www.lrz.de](http://www.lrz.de)). FLL is supported by the National Key R&D Program of China through grant 2020YFC2201400 and the Key Program of NFSC through grant 11733010 and 11333008. YC acknowledges the support of the Royal Society through a University Research Fellowship. For the purpose of open access, the author has applied a Creative Commons Attribution (CC BY) licence to any Author Accepted Manuscript version arising from this submission.

## Supplementary Material

### Understanding the optimal weights

To understand the physics for the optimal weights, we turn to look at their two dependants, halo mass and cosmic-web environment,  $(M, Env)$ .

(i) On the axis  $M$ : we can see from the lower panels of Figure 4 that high-mass halos are given more weights. This is consistent with what was found in [3, 5], and the trend is the same among all four different cosmic-web environments. This is expected as in the extreme case where all matter collapses into halos, mass weighting must be the optimal. In practice, we have a low-mass cutoff, therefore, the optimal weight function versus halo mass has a shallower slope than the mass weighting case – more weight is given to the low-mass halos to account for the missing mass below the cutoff mass. The general trend is that it is the optimal to give massive halos more weight. Given that the linear bias of halos  $b(M)$  increases with halo mass and the slope of  $b(M)$  is steeper for the massive halos i.e., the most massive halos have the highest amplitude of clustering and the highest signal-to-noise in the Poisson model. They are indeed the most ‘valuable’ for the reconstruction.

(ii) On the axis of  $Env$ : for halos in a fixed mass bin, we find that void-halos is given significantly more weights, followed by sheets, filaments, and knots, but the weights correlated strongly with the number fraction of halos in these four cosmic-web environments (top-left panel of Figure 4). This indicates that the weights are driven primarily by the number of halos in each bin (top-middle panel of Figure 4). Intuitively, we do expect that the more halos in the environmental bin, the more information about the underlying matter density field that bin may contain, and therefore more weight should be given to the bin that has the most numerous halos. However, a further question is, does the weight per halo follow the same trend i.e., is a void-halo weighted more significantly than a knot-halo? To test this, we take the ratio between the weights and the number of halos in each environmental bin, shown in the top-right panel of Figure 4. We find that the picture is mixed: For the low-mass bins, each void-halo is indeed weighted more, followed by sheets, filaments, and knots; This is consistent with our expectation that low-mass halos in a void environment may have the largest dynamical range of formation time, hence a stronger assembly bias. This makes void-halos more ‘valuable’ for the reconstruction, and thus their weight is larger. For the highest mass bin, however, the trend is of the opposite, with each knot-halo being weighted most. We think that this is the combined consequence of the wider dynamical range in halo mass in that bin, and that knot-halos are the most massive ones. As we recall from (i), along the axis of halo mass, it is

preferable to up-weight massive halos as they are more ‘valuable’. Also, massive halos typically form in the late-time Universe, with relatively few of them in voids, and most of them are in knots, and may not sample very well other cosmic-web environments – a relatively narrow range of cosmic-web environment. Both these factors make it preferable to up-weight knot-halos.

To further illustrate the above points, we made a two mass-bin case presented in Figure 5. We can see that for the low-mass bin, the range of halo mass is much narrower, further splitting it into finer mass bins does not help for the reconstruction (bear in mind that the function of  $b(M)$  is also relatively flat in this mass range). Therefore, adding the environmental dependence significantly improves the cross-correlation coefficients. For the high-mass bin, the range of mass is a lot wider (also  $b(M)$  is a relatively steep function of  $M$  in this mass range). Therefore, splitting the sample in mass helps to improve the reconstruction more significantly, and the improvement with the additional split in the environment is relatively minor.

In summary, when considering the weight of each halo, mass and environment can be seen as two competing factors. For high-mass halos, due to the steep relationship of  $b(M)$ , and the narrower range in formation time, mass-weighting is winning over the environmental factor; for low-mass halos, the opposite is true. With an almost flat function of  $b(M)$ , and a wider range in formation time (approximate as a wider range of cosmic-web environment being sampled), it is preferable to give halos in low-density (voids) environments more weight.

---

\* cai@roe.ac.uk

† flonglong@mail.sysu.edu.cn

- [1] A. Dekel and O. Lahav, *app* **520**, 24 (1999), arXiv:astro-ph/9806193 [astro-ph].
- [2] U. Seljak and M. S. Warren, *maras* **355**, 129 (2004), arXiv:astro-ph/0403698 [astro-ph].
- [3] Y.-C. Cai, G. Bernstein, and R. K. Sheth, *maras* **412**, 995 (2011), arXiv:1007.3500 [astro-ph.CO].
- [4] U. Seljak, N. Hamaus, and V. Desjacques, *pri* **103**, 091303 (2009), arXiv:0904.2963 [astro-ph.CO].
- [5] N. Hamaus, U. Seljak, V. Desjacques, R. E. Smith, and T. Baldauf, *pre* **82**, 043515 (2010), arXiv:1004.5377 [astro-ph.CO].
- [6] H.-J. Seo and D. J. Eisenstein, *app* **665**, 14 (2007), arXiv:astro-ph/0701079 [astro-ph].
- [7] R. E. Angulo, C. M. Baugh, C. S. Frenk, and C. G. Lacey, *maras* **383**, 755 (2008), arXiv:astro-ph/0702543 [astro-ph].
- [8] M. White, *arXiv e-prints*, arXiv:1004.0250 (2010), arXiv:1004.0250 [astro-ph.CO].
- [9] J. D. Cohn, M. White, T.-C. Chang, G. Holder, N. Padmanabhan, and O. Doré, *maras* **457**, 2068 (2016), arXiv:1511.07377 [astro-ph.CO].
- [10] F. Lepori, E. Di Dio, M. Viel, C. Baccigalupi, and R. Dur-  
rer, *cap* **2017**, 020 (2017), arXiv:1606.03114 [astro-ph.CO].
- [11] Z. Ding, H.-J. Seo, Z. Vlah, Y. Feng, M. Schmittfull, and F. Beutler, *maras* **479**, 1021 (2018), arXiv:1708.01297 [astro-ph.CO].
- [12] A. Patej and D. J. Eisenstein, *maras* **477**, 5090 (2018), arXiv:1709.03514 [astro-ph.CO].
- [13] H.-J. Seo, A. Ota, M. Schmittfull, S. Saito, and F. Beutler, *maras* **511**, 1557 (2022), arXiv:2106.00530 [astro-ph.CO].
- [14] S. Bonoli and U. L. Pen, *maras* **396**, 1610 (2009), arXiv:0810.0273 [astro-ph].
- [15] Y.-C. Cai and G. Bernstein, *maras* **422**, 1045 (2012), arXiv:1112.4478 [astro-ph.CO].
- [16] X. Yang, P. Zhang, J. Zhang, and Y. Yu, *maras* **447**, 345 (2015), arXiv:1309.2474 [astro-ph.CO].
- [17] M. Eriksen and E. Gaztañaga, *maras* **480**, 5226 (2018), arXiv:1508.00035 [astro-ph.CO].
- [18] S. Zhou, P. Zhang, and Z. Chen, *maras* **523**, 5789 (2023), arXiv:2304.11540 [astro-ph.CO].
- [19] R. Ma, P. Zhang, Y. Yu, and J. Qin, *arXiv e-prints*, arXiv:2306.15177 (2023), arXiv:2306.15177 [astro-ph.CO].
- [20] T. Baldauf, U. Seljak, R. E. Smith, N. Hamaus, and V. Desjacques, *pre* **88**, 083507 (2013), arXiv:1305.2917 [astro-ph.CO].
- [21] D. Ginzburg, V. Desjacques, and K. C. Chan, *pre* **96**, 083528 (2017), arXiv:1706.08738 [astro-ph.CO].
- [22] Y. Liu, Y. Yu, and B. Li, *apps* **254**, 4 (2021), arXiv:2012.11251 [astro-ph.CO].
- [23] O. Friedrich, A. Halder, A. Boyle, C. Uhlemann, D. Britt, S. Codis, D. Gruen, and C. Hahn, *maras* **510**, 5069 (2022), arXiv:2107.02300 [astro-ph.CO].
- [24] L. Gao, V. Springel, and S. D. M. White, *maras* **363**, L66 (2005), arXiv:astro-ph/0506510 [astro-ph].
- [25] L. Gao and S. D. M. White, *maras* **377**, L5 (2007), arXiv:astro-ph/0611921 [astro-ph].
- [26] O. Hahn, C. Porciani, C. M. Carollo, and A. Dekel, *maras* **375**, 489 (2007), arXiv:astro-ph/0610280 [astro-ph].
- [27] R. A. Skibba and A. V. Macciò, *maras* **416**, 2388 (2011), arXiv:1103.1641 [astro-ph.CO].
- [28] Y. Chen, H. J. Mo, C. Li, H. Wang, X. Yang, Y. Zhang, and K. Wang, *app* **899**, 81 (2020), arXiv:2003.05137 [astro-ph.GA].
- [29] M. Borzyszkowski, C. Porciani, E. Romano-Díaz, and E. Garaldi, *maras* **469**, 594 (2017), arXiv:1610.04231 [astro-ph.CO].
- [30] S. Ramakrishnan, A. Paranjape, O. Hahn, and R. K. Sheth, *maras* **489**, 2977 (2019), arXiv:1903.02007 [astro-ph.CO].
- [31] P. Mansfield and A. V. Kravtsov, *maras* **493**, 4763 (2020), arXiv:1902.00030 [astro-ph.CO].
- [32] <https://netlib.org/lapack>.
- [33] A. Klypin, G. Yepes, S. Gottlöber, F. Prada, and S. Heß, *maras* **457**, 4340 (2016), arXiv:1411.4001 [astro-ph.CO].
- [34] P. S. Behroozi, R. H. Wechsler, and H.-Y. Wu, *app* **762**, 109 (2013), arXiv:1110.4372 [astro-ph.CO].
- [35] J. E. Forero-Romero, Y. Hoffman, S. Gottlöber, A. Klypin, and G. Yepes, *maras* **396**, 1815 (2009), arXiv:0809.4135 [astro-ph].
- [36] K. S. Dawson *et al.*, *aj* **145**, 10 (2013), arXiv:1208.0022 [astro-ph.CO].
- [37] S. Alam *et al.*, *pre* **103**, 083533 (2021), arXiv:2007.08991 [astro-ph.CO].

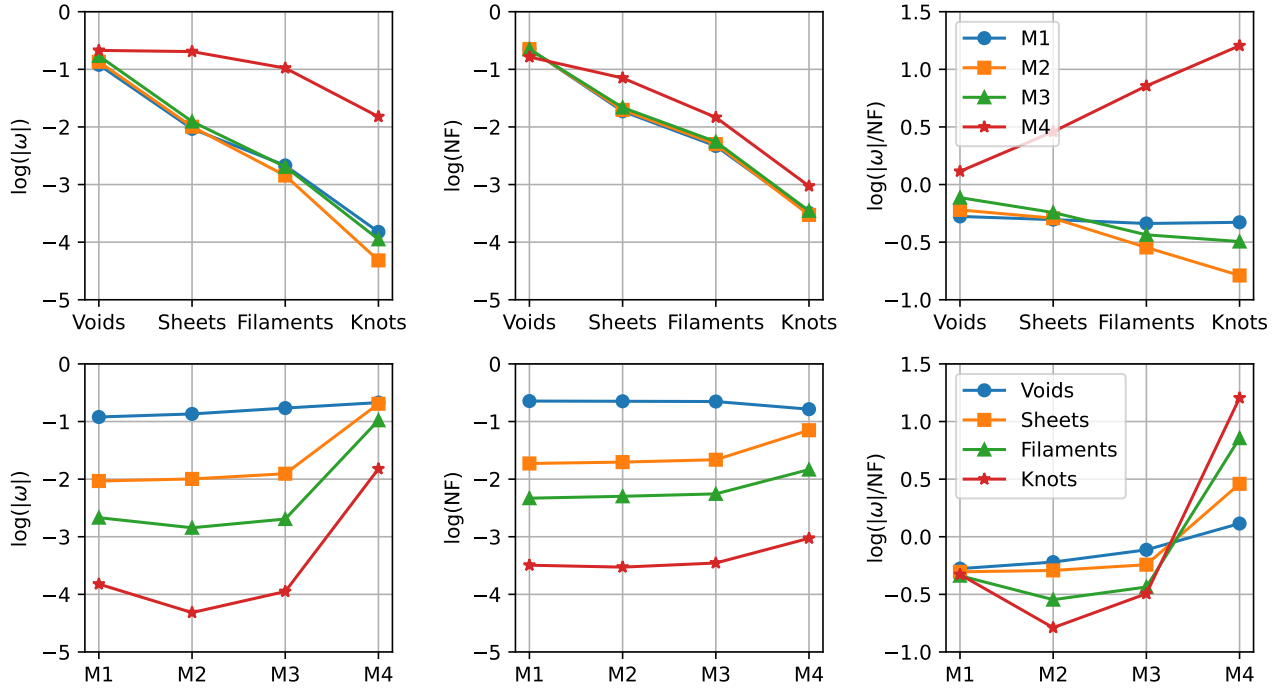


FIG. 4. Optimal weight and number fraction of halos for the  $4 \times 4$  cases i.e., four mass bins and four environmental bins. Top: environmental dependence after projecting over halo mass; Bottom: mass dependence after projecting over environments. Left: total weight given to each environmental/mass bin; Middle: number fraction of halos; Right: weight per halo. The threshold for cosmic-web classification,  $\lambda_{th} = 17.5$  has been optimized.

- [38] DESI Collaboration *et al.*, arXiv e-prints , arXiv:1611.00036 (2016), arXiv:1611.00036 [astro-ph.IM].
- [39] J. Jasche and G. Lavaux, *aap* **625**, A64 (2019), arXiv:1806.11117 [astro-ph.CO].
- [40] H. Wang, H. J. Mo, X. Yang, Y. P. Jing, and W. P. Lin,

- app* **794**, 94 (2014), arXiv:1407.3451 [astro-ph.CO].
- [41] M. Schmittfull, M. Simonović, V. Assassi, and M. Zaldarriaga, *pre* **100**, 043514 (2019), arXiv:1811.10640 [astro-ph.CO].
- [42] A. Junzhe Zhou and S. Dodelson, arXiv e-prints , arXiv:2304.01387 (2023), arXiv:2304.01387 [astro-ph.CO].

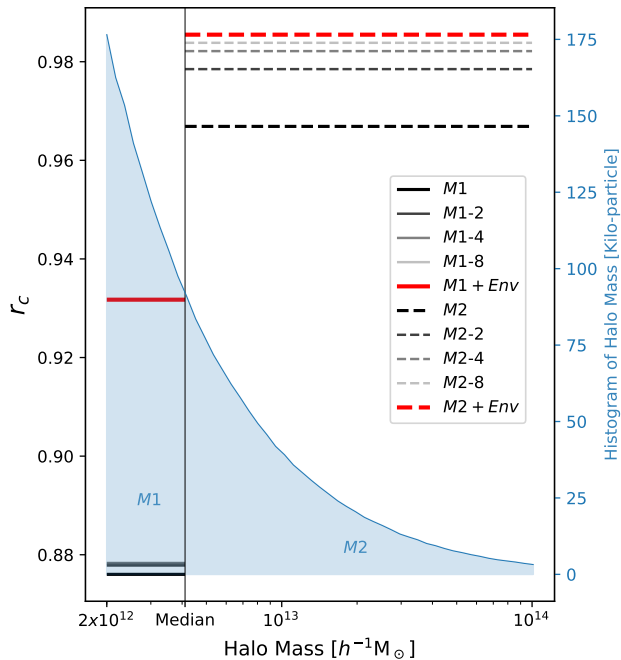


FIG. 5. Comparing the effect of environment in two different mass bins. The y-axis on the left shows the cross-correlation coefficient  $r_c$ ; the y-axis on the right indicates the histogram of halo mass with 50 logarithm mass bins. For visual clarity, we truncated the high-mass end at  $10^{14}M_\odot$  for the plot. The halo catalogue is initially partitioned into two equal-number bins, denoted as  $M1$  and  $M2$ , separated by the vertical line in the plot. We then computed  $r_c$  between  $M1$ ,  $M2$ , and the matter density field  $\delta_m$ , respectively, shown in the black-solid and black-dash lines. Within  $M1$  and  $M2$ , we further divide each bin into 2, 4, 8 bins and use the mass-dependent information to optimize  $r_c$ , shown in fainter horizontal lines as indicated in the legend. Additionally, we split both the  $M1$  and  $M2$  samples into four environmental bins, with the optimized environmental threshold value of  $\lambda_{\text{th}} = 12.5$ . The corresponding optimized  $r_c$  are shown in the red-solid line for  $M1 + Env$  and the red-dash line for  $M2 + Env$ . For the low-mass bin  $M1$ , using the mass information only provides little additional gain for the reconstruction;  $M1 + Env$  improves  $r_c$  by  $\sim 5\%$ , and so the information about the environment plays a dominant role. For the high-mass bin  $M2$ , reconstruction with the environmental information is slightly better, providing only an additional gain of  $\sim 2\%$  for the reconstruction.



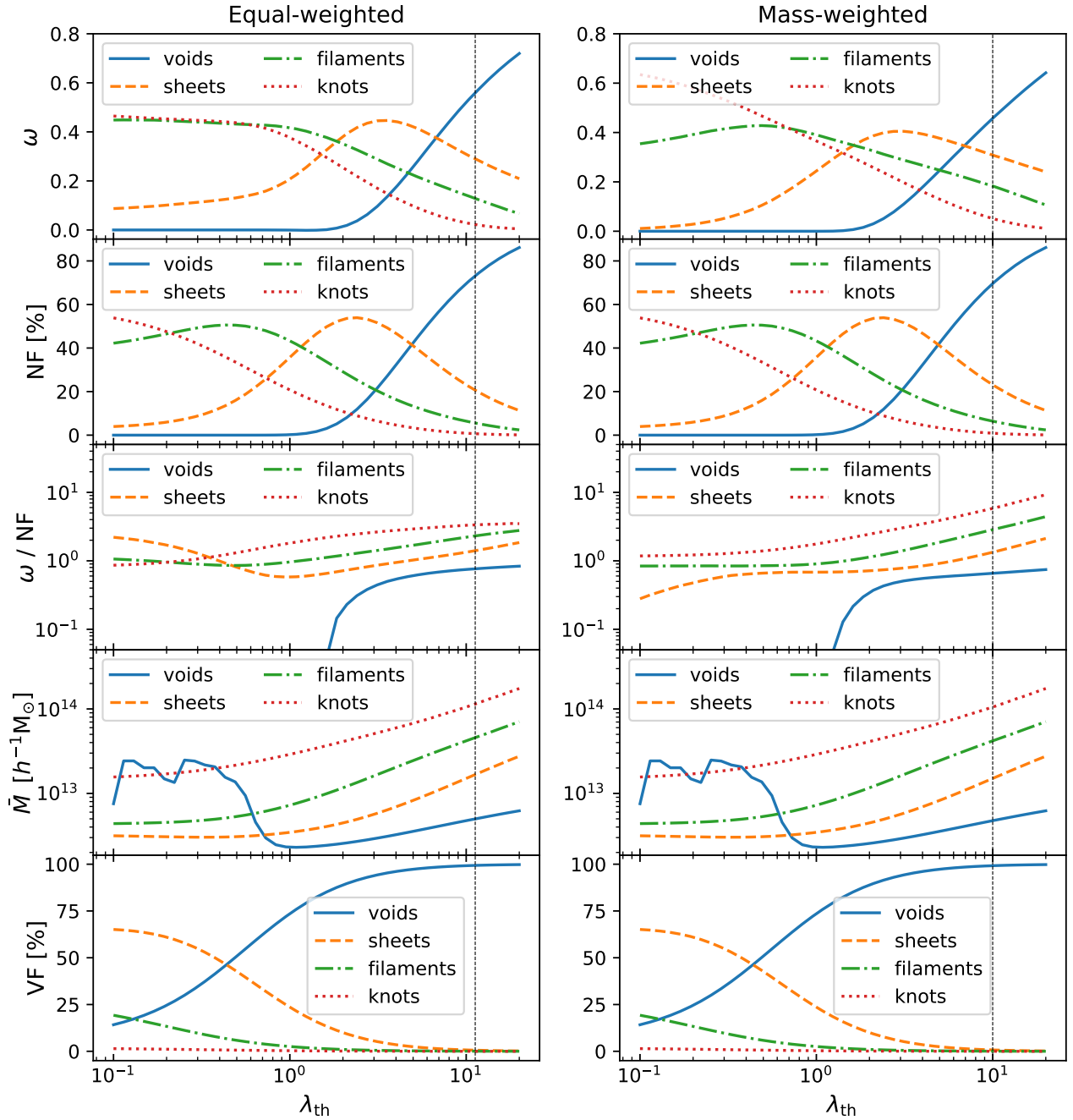


FIG. 6. Various quantities as a function of the threshold value  $\lambda_{\text{th}}$  for cosmic-web classification. The first row: optimal weight for each environmental bin; the second row: the number fraction (NF) of halos in each bin; the third row: the weight per halo; the fourth row: the mean mass of halos in each bin; the fifth row: the volume fraction (VF) classified into each cosmic-web type. Left: halos are treated equally – equally weighted; Right: halos are weighted by their mass. The vertical gray line indicates the optimal  $\lambda_{\text{th}}$  at which  $r_c$  is maximized.

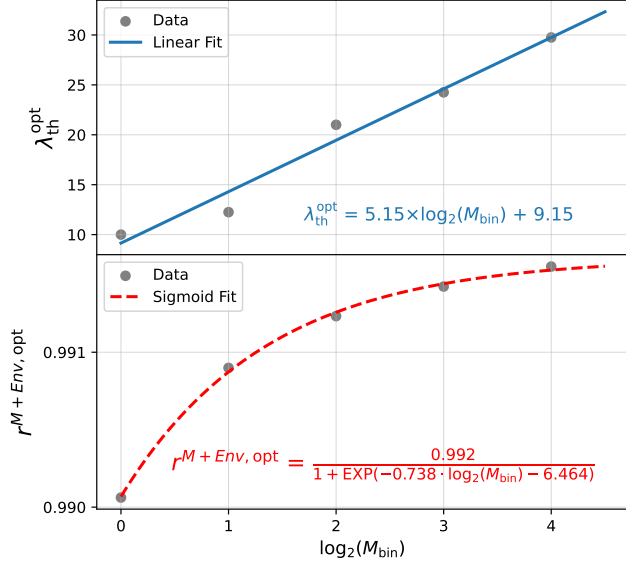


FIG. 7. Top: the optimal threshold value  $\lambda_{\text{th}}$  at which the correlation coefficient  $r_c$  is maximized as a function of the number of halo mass bins  $M_{\text{bin}}$ . The data points are measurements from the simulation, with the best-fit function shown in the legend. Bottom: the corresponding maximal  $r_c$  achieved with the optimal  $\lambda_{\text{th}}$  values from the top. A best-fit function is also shown in the legend.